BMES BIOMEDICAL ENGINEERING SOCIETY

Cyclic Mechanism Affects Lumbar Spine Creep Response

Elizabeth D. Dimbath[1] · Concetta Morino[1,2] · Shea Middleton[1] · Jason Kait[1] · Maria Ortiz-Paparoni[1] ·
Theodore A. Slotkin[3] · Jason F. Luck[1] · Cameron R.'Dale' Bass[1,2,4]

Abstract
Purpose This study aims to explore how cyclic loading influences creep response in the lumbar spine under combined flexion-compression loading.
Methods Ten porcine functional spinal units (FSUs) were mechanically tested in cyclic or static combined flexion-compression loading. Creep response between loading regimes was compared using strain-time histories and linear regression. High-resolution computed tomography (μCT) visualized damage to FSUs. Statistical methods, ANCOVA and ANOVA, assessed differences in behavior between loading regimes.
Results Cyclic and static loading regimes exhibited distinct creep response patterns and biphasic response. ANCOVA and ANOVA analyses revealed significant differences in slopes of creep behavior in both linear phases. Cyclic tests consistently showed endplate fractures in μCT imaging.
Conclusion The study reveals statistically significant differences in creep response between cyclic and static loading regimes in porcine lumbar spinal units under combined flexion-compression loading. The observed biphasic behavior suggests distinct phases of tissue response, indicating potential shifts in load transfer mechanisms. Endplate fractures in cyclic tests suggest increased injury risk compared to static loading. These findings underscore the importance of considering loading conditions in computational models and designing preventive measures for occupations involving repetitive spinal loading.

Keywords Creep response · Lumbar spine · Mechanical testing · Combined loading · Cyclic loading

Introduction

Low back pain (LBP) affects 50–80% of adults during their lifetime [1]. Occupational ergonomics such as heavy lifting, repetitive loading, and whole-body vibrations are well-established risk factors for LBP [2–5]. Additionally,

✉ Elizabeth D. Dimbath
elizabeth.dimbath@duke.edu

1 Department of Biomedical Engineering, Duke University, 101 Science Dr, 1427 FCIEMAS Bldg, Box 90281, Durham, NC 27708, USA

2 Department of Mechanical Engineering and Material Science, Duke University, Durham, NC 27708, USA

3 Department of Pharmacology and Cancer Biology, Duke University School of Medicine, Durham, NC 27710, USA

4 Department of Biomedical Engineering, Wayne State University, Detroit, MI, USA

previous injury heightens the risk of LBP, creating a recurring injury cycle [6]. Even with known risk factors, there is a weak correlation between LBP symptoms and identifiable pathology in diagnostic imaging [7], leaving about 80% of LBP cases diagnosed as non-specific [8]. The non-specific diagnoses, combined with the diverse causes of LBP, make prevention and treatment challenging [2, 8, 9]. Although the etiology of LBP is largely unknown and likely multifactorial, injury and disc degeneration are expected to play a role [10, 11]. Thus, understanding the mechanisms underlying spinal injury and failure is important for developing effective mitigation strategies for LBP.

Mechanical fatigue potentially plays a pivotal role in LBP scenarios due to the repetitive loading nature in occupations such as long-distance drivers and aircraft operators [12, 13]. Fatigue testing shows increased lumbar injury with combined flexion and compression loading, compared to axial compression alone [14, 15]. The inclusion of flexion is important as loading in daily and occupational settings is rarely purely axial; loading of the spine often

occurs with some level of bent posture [16–18]. Static flexion decreases the time to failure of spinal segments, reduces the compressive tolerance of the intervertebral disc (IVD) by 23–47% [19, 20], and results in greater fluid loss from the IVD than neutral postures [17, 21]. Moreover, the addition of repetitive loading accelerates tissue failure, increasing the risk of injury compared to static loading under axial compression [13, 22–24].

The lumbar spine exhibits viscoelastic deformation under compressive loads, which is primarily attributed to the vertebral endplates and IVD components [25, 26]. However, this behavior is dependent on both fluid flow and intrinsic tissue material response [17, 27], making mechanical characterization under various loading conditions challenging. Tissue changes in this region, such as annulus tears, nucleus pulposus herniation, disc dehydration, and endplate fractures, among others, are associated with disc degeneration and back pain [10, 28].

IVD degeneration is associated with an increased creep rate in spinal tissues [29–31]. However, understanding how creep response varies across loading profiles is limited, especially for cyclic combined flexion-compression and spinal posture, since both may exacerbate spine failure mechanisms [21]. This raises questions about whether postures such as sitting quasistatically in a flexed forward position, such as at a desk or shock isolated seat, produce fundamentally different responses (or risk of back pain) than those flexed forward with applied oscillatory load, such as in an offroad or military vehicle, where there is whole-body vibration. Additionally, it prompts consideration of whether findings from injury studies conducted under quasistatic conditions can be extrapolated to those exposed to cyclic loading.

Previous studies suggest that cyclic combined loading may be a potential risk factor for increasing LBP [20, 32, 33], yet comparisons are challenging due to the various loading scenarios used in lumbar mechanical testing. Specifically, gaining insights into the variations in creep response under flexion-compression loading in cyclic and static scenarios will enhance the accuracy of computational modeling tools in predicting injuries. These injury prediction models can provide valuable information for developing strategies to mitigate LBP and injury in populations exposed to particular loading patterns. Hence, a comparative analysis of creep response is a crucial step toward understanding the mechanism and progression of injury and pain in the lumbar spine.

This study evaluates the effects of the cyclic mechanism on lumbar spine mechanical behavior under combined flexion-compression loading scenarios. Testing porcine lumbar spinal units under both cyclic and static combined loading regimes *ex vivo* provides a comparison of the mechanical response over the test duration to vertebral endplate failure. Understanding the tissue mechanical response under these two loading regimes will offer insight into the mechanistic progression of lumbar injury and LBP.

Materials and Methods

Specimen Preparation

Porcine spines were used as an animal model in this study as they are similar in size and structural response to human spines [33, 34]. Ten porcine functional spinal units (FSUs) from four male Yorkshire pigs (procured from post-mortem specimens of the Duke Division of Laboratory Animal Resources) were used in this study. The porcine cadaver spines used in this study were harvested from animals euthanized as part of a separate IACUC approved protocol at Duke University. The spines were unaffected by the IACUC research protocol, and thus viable for the current study and exempt from direct IACUC approval. FSUs include two vertebral bodies, an intervertebral disc, and osteoligamentous components. At the time of harvest, pigs weighed 70–80 kg. Lumbar spines were separated into osteoligamentous FSUs with the surrounding muscles and tendons removed. Pigs have a variable number of lumbar vertebrae, typically five or six [35]. Thus, depending on the number of lumbar vertebrae in each spine, FSUs included vertebral bodies from the lowermost thoracic vertebra down to L6 (Table 1). FSUs containing S1 were not included due to the known increased material stiffness at this level [36]. Following harvest, FSUs were frozen (−20 °C) until test preparation.

Prior to testing, FSUs were imaged using high-resolution computed tomography (μCT) (Nikon XTH 225 ST). μCT images were used to calculate initial endplate-to-endplate distance (EP distance), endplate area, and examine the FSUs for any pre-existing injury. EP distance and endplate area were found using ImageJ (U.S. National Institutes of Health,

Table 1 Pig test specimen information

| Pig	Mass (kg)	Test #	Loading regime	Spinal level	Endplate area (mm^2)
1	73.5	1a	Cyclic	L3–L4	603
		1b	Static	L1–L2	595
		1c	Static	L5–L6	564
2	70	2a	Cyclic	L5–L6	611
		2b	Static	L3–L4	645
		Control	–	L1–L2	640
3	80	3a	Cyclic	L2–L3	556
		3b	Static	L4–L5	561
4	77	4a	Cyclic	TX–L1	592
		4b	Static	L4–L5	635

Bethesda, Maryland, USA). The porcine lumbar vertebrae have well-defined boundaries between the endplates and vertebral bodies. Thus, the EP distance was defined as the average distance between the inferior endplate of the superior vertebral body and the superior endplate of the inferior vertebral body. The average EP distance was calculated from nine measurements: three lateral measurements (left, middle, right) in each of three coronal slices (anterior, middle, posterior). EP distance was used to calculate the engineering creep strain. The cross-sectional area was measured on an axial view of the endplate to find the endplate area. If endplate damage or degradation of IVD tissues was observed in pre-test μCT the specimen was excluded from the study.

Mechanical Testing

Specimens were loaded into a biaxial test system for combined flexion-compression loading. The system consisted of two servo-hydraulic materials testing systems (MTS, Eden Prairie, MN, USA). Two actuators applied the combined loading pattern: an axial actuator located inferior to the specimen applied compression in load control and a rotational actuator, affixed to the side of the specimen, applied independent flexion in angular displacement control. Combined flexion-compression loading results in peak loads that combine the applied compressive load with the loading due to angular displacement with the application of flexion. Sampling frequency of data was 2 kHz. A 6-axis load cell, an AMTI MC5-6-500, was affixed superior to the specimen

and measured bending moments during the tests. An additional 6-axis load cell, a Denton 1716A, was mounted below the specimen in line with the axial actuator and measured the axial forces during the tests. Additionally, a linear variable differential transformer (LVDT) located inferior to the specimen (internal axial LVDT of the MTS system) tracked axial displacements from the bottom of the specimen over the duration of the test and an internal rotary variable differential transformer (RVDT) mounted to the side of the specimen collected angular displacement of the superior end of the specimen during the test. An environmental chamber surrounded the testing system, providing test conditions to simulate *in vivo* temperature and humidity (37 °C and 100% humidity). A preload was not applied to the specimens prior to testing since specimens were not exposed to procedures known to change hydration (i.e. saline bath). The specimens were acclimated to the simulated in vivo conditions prior to loading. Fig. 1 depicts the test setup with placement of the specimen along with the load cells, actuators, and transformers.

FSUs were fastened to the test apparatus at the superior and inferior vertebral bodies. Screws and k-wires were secured into the superior and inferior ends of the FSU. Then, the screws and k-wires were embedded in polymethylmethacrylate (PMMA) to provide rigid attachment points and increase surface area for casting materials. The PMMA was cast using a fast-curing resin (Golden West Mfg., Inc., Grass Valley, CA 95945) in aluminum mounting cups that were affixed to the test apparatus. The superior mounting cup
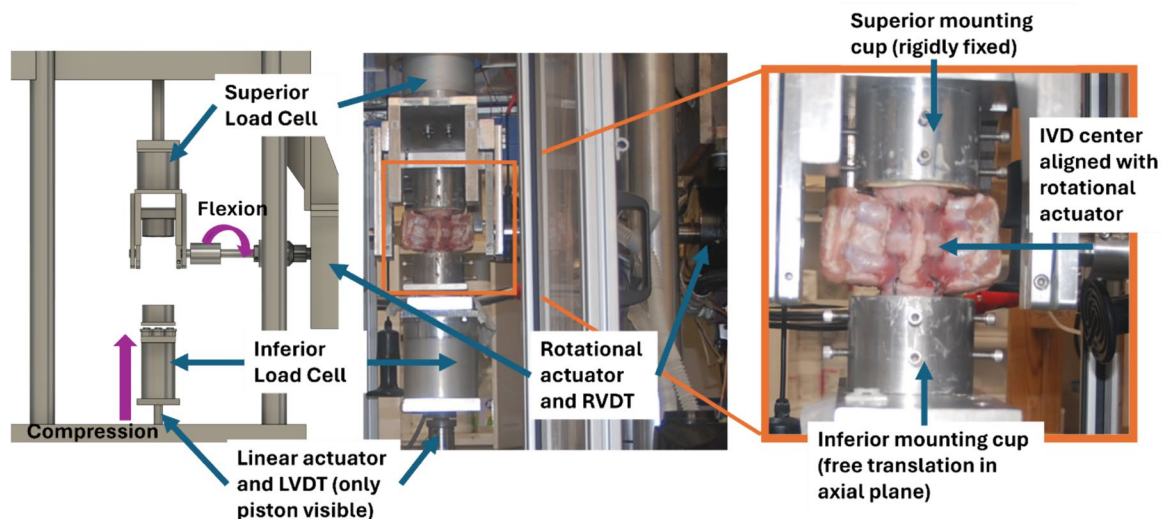

Fig. 1 Overview of experimental test setup. Schematic on left (adapted from: Schmidt-unpublished) shows placement of load cells, actuators and transformers on MTS system with location of applied flexion and compression. Middle image is picture of test setup with specimen mounted in test apparatus and enclosed by environmental chamber (chamber door open). Magnified image shows specimen fixed in mounting cups with the upper end rigidly mounted to the test apparatus and the inferior mounting cup affixed to a plate with ball bearings to allow for free translation in horizontal plane. The IVD is aligned with the shaft of the rotational actuator defining the center of rotation

was rigidly mounted to the test apparatus while the inferior mounting cup, while restricted in the z-axis, was free to move in the lateral and anterior/posterior directions during testing. For proper alignment, FSUs were positioned at the center of the mounting cups, ensuring that the axial plane of the IVD was perpendicular to the direction of compressive force and centered with the axis of flexion rotation. This ensured consistent posture between specimens.

FSUs underwent one of two different combined flexion-compression loading regimes: cyclic or static. Four FSUs were loaded under the cyclic regime, five underwent static loading and one served as a control. The control specimen was prepared in the same manner as test specimens and placed in the environmental chamber for the same duration as a typical test. The control was used to ensure the experimental setup was not responsible for differences observed in tested specimens. FSUs were paired such that, from a single porcine spine, one FSU underwent cyclic loading and at least one underwent static loading. Each FSU was only tested once under one loading condition. The cyclic loading profile consisted of a 1 Hz sinusoidal compression wave combined with a 1 Hz offset flexion ramp ranging from 0 to 6° [37] (Fig. 2). This loading pattern was modeled from high-speed boat operators undergoing vertical underbody loads resulting in compression and delayed flexion [16] but can be generalized to other occupational exposures. Peak loads used in this study are typical of high-speed watercraft, helicopter, and fast jet occupants, which typically experience ~ 1–6 g and up to 15 g of vertical accelerated loading. The use of 0–6° of flexion is considered a more extreme form of flexion-compression loading equal to about 45° of total torso flexion [20]. This flexion range is within the normal range of motion for both humans and pigs. The angular displacement is applied when the compressive load reaches 80% of the peak load to simulate this delayed flexion loading. Directly after testing, FSUs were removed from the test fixture and frozen (− 20°C). FSUs underwent μCT imaging after freezing. Post-test μCT scans were used to visualize
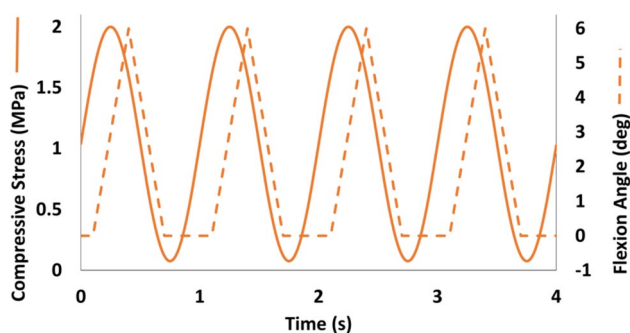
Fig. 2 Oscillatory loading profile with 1 Hz sinusoidal compression and offset 1 Hz flexion angle from 0 to 6°. Initial ramp to prescribed load not shown

injury outcomes and determine the location and type of injury.

The axial actuator loaded FSUs under force control. The flexion angle was varied between 0 and 6° by the rotational actuator under displacement control. Peak compressive loads varied between FSUs and were scaled by endplate area to provide equivalent applied stress to the IVD. Endplate areas for each test specimen can be found in Table 1. The applied stress was the combined stress due to axial compression and flexion moments through the application of a flexion angle. This was measured by the inferior load cell as force. A peak applied stress level of 4.15 MPa was chosen based on an injury risk profile developed in a previous study for the same loading regime [38]. This peak stress level is the maximum stress applied to the FSU due to the combined axial compression and flexion. The applied stress is high for physiological loading but would be expected to result in failure in hours rather than days as would be the case with lower stress levels. Resulting peak loads varied from 2300 to 2530 N. A baseline load of 76 N was applied to account for the minimum compressive load experienced by the lumbar spine without additional external load. FSUs were loaded past failure, with failure defined by an inflection in the displacement-time history. Failure is characterized by endplate fracture in this test series. This inflection indicates changes in the mechanical properties of the specimen from damage [33]. The inflection was visually identified from the displacement-time history during testing then failure was verified with μCT. Total test durations ranged from 1.2 to 8.1 hrs., with an average of 4.0 hrs (SD = 2.5).

For the static loading regime, the axial compressive force and flexion angle were held constant over the entire test duration. The applied compressive force scaled by endplate area also provided 4.15 MPa of stress. The load was ramped over 20 s, first rotating at the superior end to the desired flexion angle then axially compressing from the inferior end. Applied force ranged from 2340 to 2680 N. Duration of static tests was based on the failure of paired cyclic tests, with static tests running until at least the time of failure in the paired cyclic test. For static tests, total loading duration ranged from 1.2 to 6.7 h, with an average of 5.3 h. (SD = 2.1).

The flexion angle for static loading was chosen based on preliminary testing that aimed to optimize static loading's primary creep response to match that seen in cyclic loading [39]. In the preliminary study, seven FSUs were tested under static and cyclic combined loading and primary creep response was compared. The same methodology, as described above, was used in the preliminary study for loading specimens in both conditions. Flexion angle in static loading scenarios of the preliminary study was varied to match the cyclic primary creep, or short duration, response. Flexion angles of 3°, 5°, and 5.5° were all tested and compared to paired cyclic tests.

Testing at 2.05 MPa applied stress with 5° flexion provided static testing parameters that resulted in similar creep behavior to cyclic tests at the same peak stress with cyclic compression and cyclic flexion from 0 to 6°. Based on these earlier findings, a constant flexion angle of 5° was selected as the flexion angle to be investigated for the static loading condition in the current study.

Data Analysis

Data was compiled as strain-time histories beginning after each specimen was ramp loaded to the desired stress level. The displacement data from cyclic tests were filtered using an 8th order phaseless low-pass Butterworth filter with a 0.1 Hz cutoff frequency to establish comparisons across the cyclic and static loading regimes. Datasets were downsampled to 2 Hz consistently across tests for ease of data analysis. Data from both loading regimes were truncated at the time of inflection in the paired cyclic test. Truncation limited analysis to creep before behavior changes due to tissue injury occurred. The engineering strain in each IVD was calculated by dividing the axial displacement by the initial EP distances determined in pre-test µCT imaging. EP distance was used for strain calculation rather than IVD height alone since deformation of the endplate into the vertebral body contributes to strain [25]. Strain was used to account for size differences between FSUs and normalized to mitigate inter-specimen variability. Strain normalization was carried out by subtracting the initial strain. The initial strain was defined as the strain directly after specimen was ramp loaded to the desired stress level. Time was log-transformed to visualize differences at longer time durations, and strain-time histories were used to compare creep response.

Statistical Analysis

Owing to multiple phases of response, different loading regimes, and time-dependent effects, data were analyzed using two statistical methods to ensure that interpretations were reliable. The first method used an analysis of covariance (ANCOVA). Since we are interested in strain response due to applied stress over the course of time, we compared the results between loading regimes using a global ANCOVA. Since ANCOVA is dependent on least squares regression, the data were linearized using the Hill equation and Hill plot (see Data Linearization in Appendix), which is applicable to biological processes that exhibit a fixed maximum response (rectangular hyperbola):

$$\log\left(\frac{Y}{1-Y}\right) = m\log(X) - b \tag{1}$$

For this study, Y corresponds to the normalized strain and X is time. In the ANCOVA analysis, the response variable was the linearized strain with factors of regression phase (phases discerned in linearization of the data; see Phase Determination in Appendix) and loading regime: either cyclic or static. Time in the log domain was the covariate. If interactions of regression phase with loading regime were identified, the data were subdivided and lower-order ANCOVA was performed. The lower-order ANCOVA permitted regression analysis to determine slope changes between loading regimes in each linear phase.

The second statistical approach for data analysis involved both linear regression and subsequent analysis of variance (ANOVA). Linear regression modeled the relationships within the data. Then ANOVA was employed to assess potential statistical differences between slope variables among the groups. A least squares linear regression was performed for each phase of each test. The resulting slope values were compared in a global ANOVA using loading regime and regression phase as the factors. This approach substantially decreased the degrees of freedom in the analysis compared to ANCOVA which accounted for every data point in the curves. Similar to the ANCOVA approach, if the interaction term between loading regime and regression phase was significant ($p < 0.05$), the data were subdivided, and lower-order ANOVA was performed. The lower-order ANOVA assessed if slopes were different between loading regimes in each linear phase ($p < 0.05$).

Results

Qualitative differences were seen in the plot of the normalized strain response between the cyclic and static loading regimes (Fig. 3). At longer time durations, the cyclic and static loading regimes showed different trends: cyclically loaded tests showed a continued increase in strain response similar to exponential response (Fig. 3a), whereas the statically loaded tests begin to taper off and appear to hit an asymptote below normalized strain values of 0.6 (Fig. 3b).

Strain linearization with the Hill transformation revealed a biphasic response for both loading regimes (Fig. 4). The linearized data show an initial period with nonlinear (curved) values followed by an initial region of linearity that leads to a second nonlinear region and then resolution to a second linear phase (Fig. 4a and b). This biphasic trend in linearization is likely due to biological changes in tissue response over the duration of the test. Hence, we considered both of the linear regions in our analysis. The initial linear region is referred to as linear phase 1 (L1), and the second is termed linear phase 2 (L2); the initial and intermediate nonlinear zones were considered to be transitional and thus were not included in the statistical analysis. The start and end points for each phase were determined using the curvature peaks in the nonlinear regions (Fig. 4a and b). The curvature

Fig. 3 Strain-time histories from porcine FSUs tested under cyclic and static loading regimes with combined flexion-compression. **a** Strain-time history of four specimens tested under cyclic combined loading, showing continued increase in strain over duration of test. **b** Strain-time history of five specimens tested under static combined loading, where strain shows decreased growth at later time points. Label numbers (1–4) correspond to specimen number and letters (a–c) correspond to tested FSU
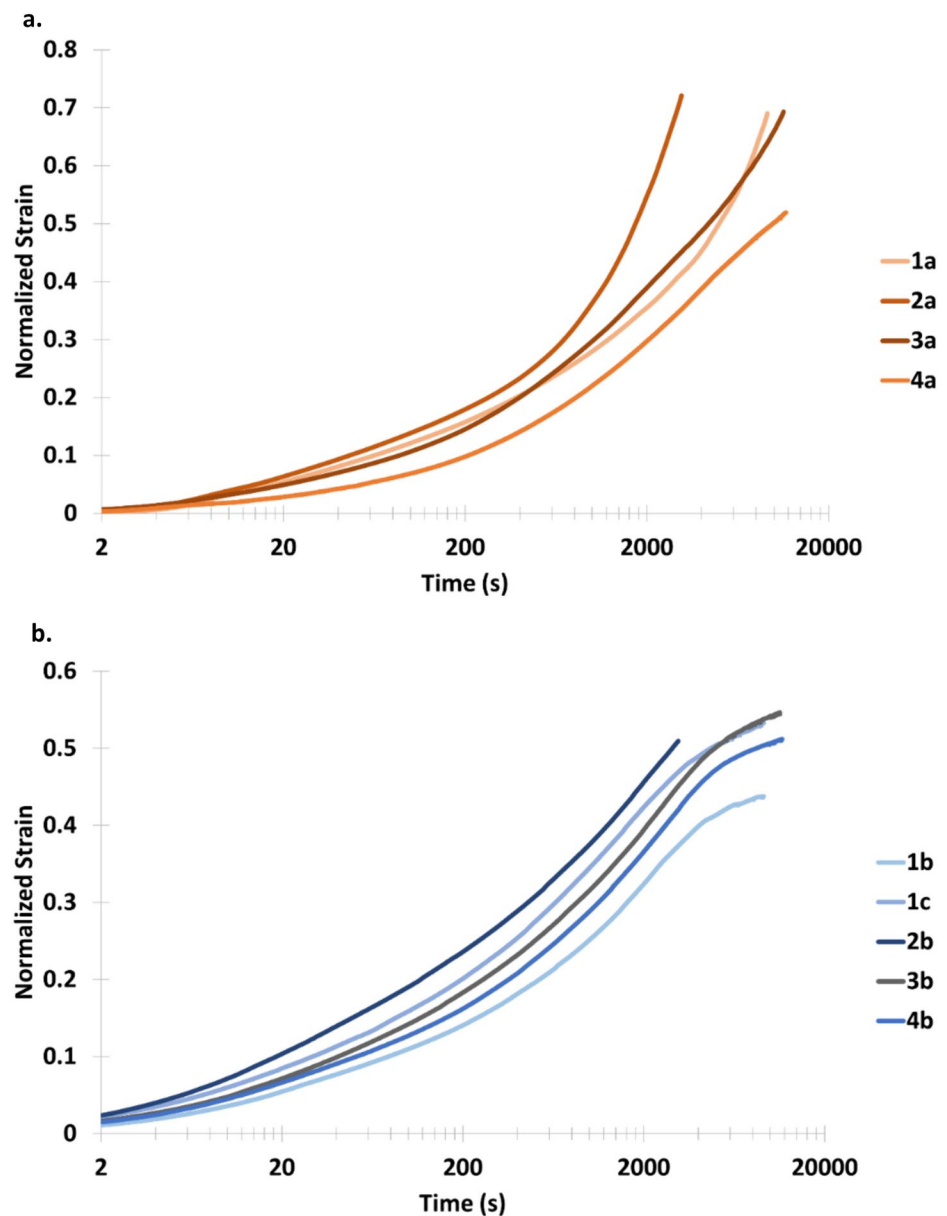
peaks were used as a basis for defining L1, the two transition phases, and L2 (see Phase Determination in appendix). With this approach, L1 and L2 had values of $R^2 \geq 0.99$ and $R^2 \geq 0.98$, respectively.

Global ANCOVA found a statistically significant ($F_{1,93840} = 2447.91$, $p < 0.001$) interaction between the regression phase and loading regime and a significant interaction between time (covariate regressor), regression phase, and loading regime. The interaction effect of the loading regime and regression phase is important as it signifies a difference in slope, or curvature, between the loading regimes with respect to each phase. A lower-order ANCOVA was carried out for each regression phase in light of the significant interaction between the regression phase and loading regime. In phase L1, at shorter durations, there was an

interaction of time on loading regime ($F_{1,18849} = 1680.49$, $p < 0.001$) (Fig. 5a). Also, in phase L2, which involves longer durations, time has an interaction effect on loading regime ($F_{1,74991} = 1006.49$, $p < 0.001$) (Fig. 5b). The significant interaction effect of time and loading regime signifies that the slopes of the strain-time histories are different between loading regimes. For visual clarity, the plots in Fig. 5 do not include the time effect due to an artifact arising from the difference in the start time of the linear phases for each test.
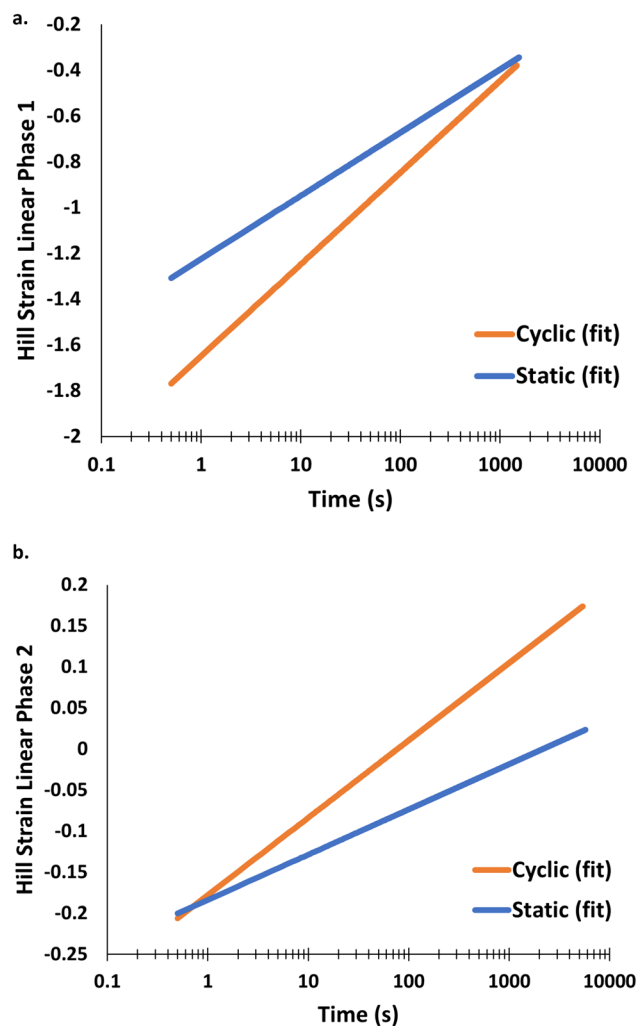
Results from linear regression followed by ANOVA were compatible with those from ANCOVA. The cyclic and static tests resulted in average regression phase L1 slopes of 0.51 (SE = 0.032) and 0.44 (SE = 0.011), respectively. In regression phase L2, the average slope for cyclic tests increased
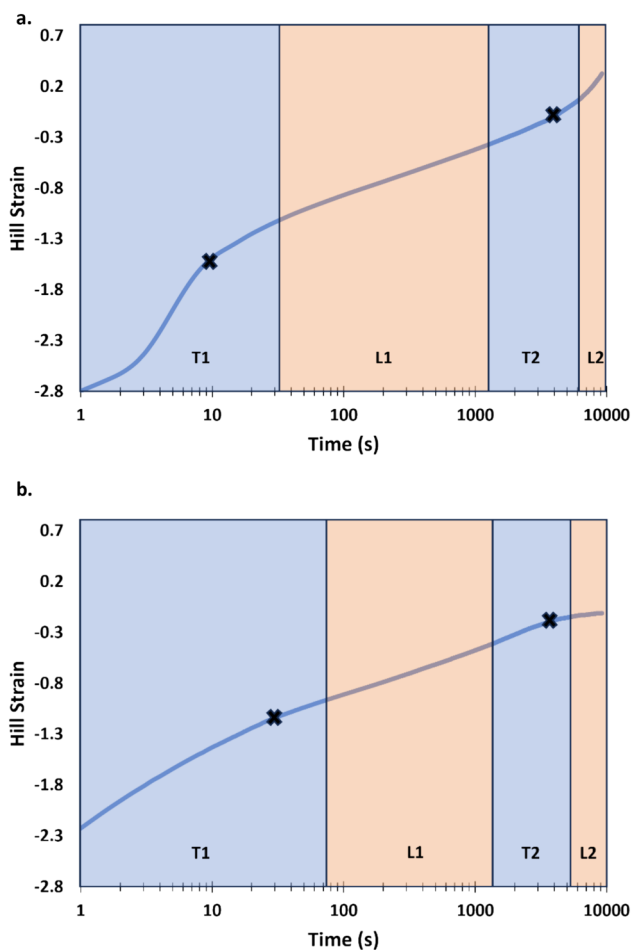
Fig. 4 Representative plots of data linearized using the Hill plot. Blue shaded regions (T1 and T2) are transition zones and orange shaded regions (L1 and L2) are first and second linear regions. X symbols denote curvature peaks that define the first linear region. **a** Hill plot of cyclic data from test 1a, all cyclic tests showed similar behavior. **b** Hill plot of static data from test 1b, all static tests showed similar behavior


Fig. 5 Slope comparison between loading regimes in each regression phase. Plots of regression fit from ANCOVA. **a** Regression phase L1 shows significant slope difference between cyclic and static loading with $p < 0.001$. **b** Regression phase L2 shows a significant slope difference with $p < 0.001$

to 1.08 (SE = 0.242), while the average slope for the static tests decreased to 0.24 (SE = 0.064). The global ANOVA comparing the slopes from linear regression found an interaction effect of the loading regime and regression phase ($F_{1,14} = 11.32$, $p < 0.005$). Based on this significant interaction, a subsequent lower-order ANOVA on each regression phase showed significance between loading regimes in phase L1 ($F_{1,7} = 6.45$, $p < 0.04$) and phase L2 ($F_{1,7} = 14.00$, $p < 0.007$) (Fig. 6). Still, after the transition point in phase L2, there is a difference in the slope of the strain-time histories between the two loading regimes.

Only cyclic tests had inflections in displacement-time histories, with no apparent inflections in static tests. Injury was verified in post-test μCT imaging, which confirmed endplate fracture in all cyclic tests (Fig. 7). The μCT images from static tests did not show visible fractures in the endplate. The

control specimen, which underwent the same experimental setup but was not loaded, did not show the discernable differences between pre-and post-test μCT images. Presence of endplate fractures was confirmed with dissection of spinal units after μCT imaging.

Discussion

Overall, cyclic and static loading showed different patterns in creep response. Statistical analyses reinforced qualitative findings of curvature differences in strain-time curves between the cyclic and static loading regimes, specifically at longer durations. Both ANCOVA and linear regression paired with ANOVA showed significance. The
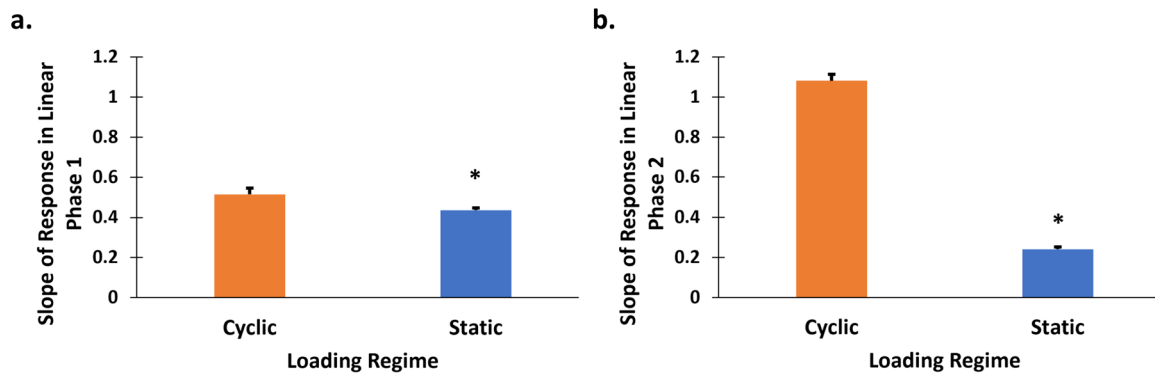
Fig. 6 The slope of creep response during each regression phase in cyclic and static loading scenarios (mean $\pm$ 1 SE). **a** Slopes in regression phase L1 are significantly different between cyclic and static loading ($F_{1,7} = 6.45$, $p < 0.04$). **b** Slopes in regression phase L2 show a significant difference between cyclic and static loading ($F_{1,7} = 14.00$, $p < 0.007$)
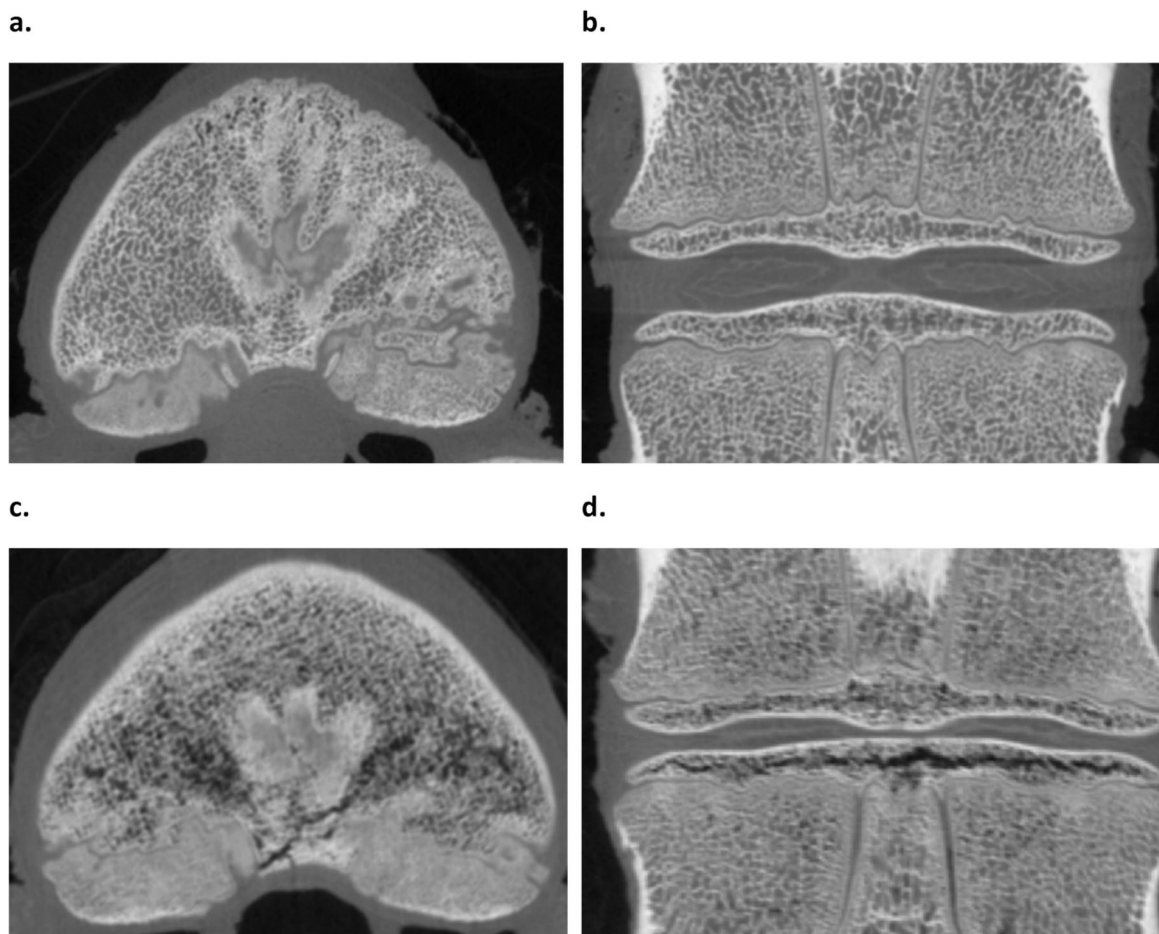
Fig. 7 Endplate fracture in cyclic test (from test 1a). **a, b** Axial and coronal view of endplate prior to testing, respectively. **c** Axial view of fracture in inferior endplate. **d** Coronal view of fracture in inferior endplate towards the posterior

results from ANCOVA, which had high degrees of freedom, were strengthened by obtaining similar results from ANOVA which had lower degrees of freedom. At shorter time durations (L1), the slope of the creep response, defined by the strain-time history, was significantly different between the cyclic and static loading regimes. The

slope of the cyclic response was slightly larger than that in the static response. This contrasts with previous work that optimized the flexion angle of the static loading condition to replicate the creep response in a cyclic loading regime at an applied stress of 2.05 MPa [39]. The current study applied high physiological stress at 4.15 MPa, thus showing that the similarity in creep response, observed with an applied stress of 2.05 MPa, in phase L1 was not observed at this higher stress level. Also, at long durations (L2) the slopes of the creep response were significantly different between the cyclic and static loading regimes with a larger difference in slopes between regimes. These differences suggest a change in tissue mechanics between loading regimes during the transition phase and phase L2.

Biphasic models have previously been used to model IVD mechanical response accounting for the interaction between fluid and solid components [40]. Utilization of such models stems from the theory that response depends on poroelastic fluid flow through the IVD and endplates as well as the viscoelastic nature of the tissues [41–44]. Observed biphasic trends in linearized data may arise from the load transfer between fluid and solid components or a shift in the interaction between different structural elements. Deformation of the endplate strongly influences initial creep behavior along with early rapid fluid flow [25]. Then late creep arises from the creep of annulus fibers and slow continued fluid loss [25]. Thus, the current findings may indicate annulus fibers and fluid loss are better adapted to static load, whereas the cyclic load produces harmful changes in the annulus fibrosus or increases the dehydration of the disc. This study is unable to discern which structural and mechanical components are responsible for the biphasic trend seen in the linearized creep response. However, the difference in behavior between loading regimes indicates important changes occur in the IVD, leading to overall changes in creep behavior and injury progression. Also, of interest is the role of the transition phase and how it affects the slope change in each loading regime. Studies coupling combined loading with dynamic imaging techniques may aid in elucidating IVD components that give rise to behavior and injury progression differences.

Mechanical overloading has been identified as a component of the onset and progression of IVD degeneration, possibly leading to LBP [27, 45, 46]. Additionally, static and dynamic loading both lead to pathological changes in the IVD, but the mechanism and progression of such changes differ [46]. Greater FSU height loss in flexed posture with cyclic axial compression compared to neutral cyclic axial compression or flexed static compression has been previously reported [14, 46]. This is qualitatively similar to the findings in the present study. However, by going a step further and comparing the curvature of the

creep responses up to endplate failure, this study provides new information on how mechanical response differs between loading regimes over the creep duration.

All cyclic tests showed indications of injury with inflections in displacement-time curves during testing with verification of injury in post-test μCT scans and dissection. Endplate fractures were visible in all cyclic post-test μCT. Conversely, the static tests did not present with endplate injury. Instead, the IVDs in the static tests all showed dark regions in the disc structure. Findings suggest increased injury risk in cyclic combined loading, particularly with respect to endplate fracture. Parkinson and Callaghan showed that load magnitude under combined loading conditions may determine the type of resulting injury, with low peak loads leading to IVD injury and vertebral fractures more likely to occur under higher peak loads [47]. When compared to previous studies applying static flexion, the combined repetitive loading profile led to injury sooner than under static flexion [47, 48]. Increased tissue strain increases the risk of injury [49], and posture is an important factor for injury risk in both static and cyclic loading [14, 46]. Further investigation is needed to classify soft tissue injury due to different loading mechanisms but results from this study indicate different injury mechanisms. The apparent asymptotic behavior in L2 in the static loading condition suggests slower progression toward injury. Thus, the lumbar spine may be more tolerant to sustained static loading for combined flexion-compression configurations, such as prolonged sitting postures, rather than repeated loading.

The findings from this study are essential in understanding fundamental IVD and endplate tissue response that is the basis of many models used to study more complex physiological responses. Such models include human body in silico models that enable testing a wide range of scenarios and conditions without the ethical concerns and time restraints that come with in vivo and in vitro testing. However, the models must accurately respond to different scenarios to translate findings from in silico models to real-world situations. Our study highlights the importance of utilizing tissue characterization from similar loading conditions as the final use case, likely including differences in poroelastic flow from oscillatory vs quasistatic conditions [42, 50]. While short-duration creep response may be similar between the loading regimes, a significant difference in creep response is seen at later durations and, thus, different injury patterns. If creep response from a static loading condition was used to decrease low back injury for motor vehicle occupants through modeling and designing seats, then the model would likely be under protective for vehicle occupants exposed to whole-body vibration. Thus, care should be taken when applying material properties to equipment design: repetitive motion scenarios should utilize cyclic tissue response.

The evident separation of creep response into distinct phases is important for the study of injury progression. The distinct phases open the door for future research to better understand how different elements of the FSU contribute to creep and biphasic behavior. One possible approach is to test FSUs for durations corresponding to each phase and then compare tissue changes using imaging techniques. This testing could help explain the differences in behavior after the transition phase, shed light on what material changes initiate the transition phase, and show differences in injury patterns between loading regimes. Furthermore, the current study elucidates the effect of cyclic mechanisms in combined loading scenarios, but similar direct comparison studies are also needed to assess the effect of posture in cyclic loading scenarios.

This study is limited by several factors. While porcine specimens are a good model for human FSUs [33, 34], there are still differences in structure and mechanical response that could lead to differences in findings. Additionally, tests were carried out in vitro, accounting mainly for the response of the IVD, endplates, vertebral bodies, and ligaments, but lack the physiological responses and repair pathways that are present in vivo. Paired cyclic and static tests came from the same pig specimen thus, spinal levels differed between conditions. To help mitigate level bias, the levels were varied between pig specimens so that each loading condition included FSUs from various levels, however some bias may still be present. Additionally, the age of specimens used in this study was unknown, only the weight. All forces were scaled to apply the same peak stress across specimens. However, additional testing would be required to determine if the findings hold true across various stress levels. Current testing at 4.15 MPa is a relatively high stress compared with quasistatic physiological loading [38] and how lower stresses would affect creep response and injury pattern is unknown. Displacement measurements were taken from the LVDT, measuring displacement in the center of the specimen. Thus, the strain is a measure of average strain across the IVD, whereas some areas may exhibit greater or smaller strain. The strain measurements in this study also only assume deformation of the IVD and endplates since they are based on EP distances. Visualizing IVD and endplates in post-test µCT give qualitative comparison of structural changes between loading conditions but further analysis is needed to quantify differences and discern physiological relevance of structural changes in IVD under static loading. Future work will aim to quantify changes in the IVD to determine what is damage to the disc and what is merely recoverable normal soft tissue changes.

This study demonstrates how cyclic loading influences the creep response under combined loading scenarios in porcine lumbar FSUs at long durations. Creep response of IVDs is often attributed to fluid flow and biphasic viscoelasticity

[44]. Thus, these results suggest that cyclic loading may alter fluid flow and increase injury risk. Additionally, under combined flexion-compression loading scenarios, the lumbar spine may be better suited for sustained static loads, especially for long-term exposure.

Appendix

Data Linearization

The data were linearized prior to running ANCOVA. Two methods were compared to determine the optimal method for linearization of the response data: the Lineweaver-Burk plot and the Hill plot. The Lineaweaver-Burk plot is a double reciprocal plot with the reciprocal of strain on the y-axis and the reciprocal of time on the x-axis. The fit using the Lineweaver-Burk plot results in an R^2 value $= 0.945$ for the test shown (Fig. 8a). Linearization using the Hill equation (Eq. 1) and Hill plot provides a better fit with R^2
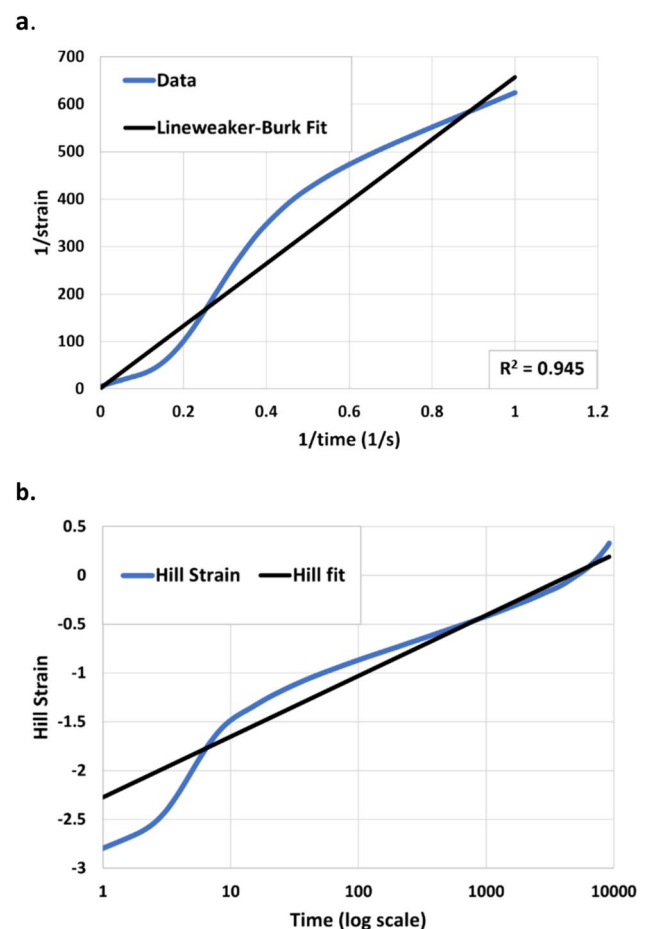
Fig. 8 Linearization of data using two methods. Results shown are for test 1a. **a** Linearization using Lineweaver-Burk plot. **b** Linearization using Hill plot

value = 0.952 (Fig. 8b). The Hill equation and Hill plot were chosen for data linearization as this method consistently provided higher R^2 values than the Lineweaver-Burk plot for each test.

Phase Determination

Linearization of data resulted in biphasic response for both loading regimes. As such, data were divided into distinct regions for statistical analysis. As stated in the text, four distinct phases are seen in the linearized data. Peaks in the curvature of the response was used to objectively define the bounds of each phase. Curvature was calculated in MAT-LAB R2022b (The MathWorks Inc., Natick, Massachusetts). First, data were filtered using a moving median filter with a window size of 700. The first derivative was computed using a central difference scheme using a 5-point stencil. 7-point and 9-point stencils were also tested but results converged using the 5-point scheme. To remove residual noise in the derivative, a Gaussian filter was applied. A Gaussian filter was also used on the second derivative, which was computed using a finite difference scheme. Using the filtered first and second derivatives, the curvature was computed:

$$k = \frac{|y\varepsilon|}{(1 + y\prime^2)^{3/2}} \tag{2}$$

Peaks from the curvature were used to define the transition phases (Fig. 9). Peaks below log time value 0.5 were removed and not considered as there are too few data points in this region to be confident in the magnitude of this peak. The highest magnitude peak above this threshold and the final peak were used to define the start and end points of each phase (Fig. 9).

These bounds represent the place of maximum curvature. To remove the curvature and only capture the linear region, the middle 60% between these two curvature bounds defined the first linear region. This was done by determining the time that signified 20% of the total time between curvature peaks and adding that amount to the lower curvature peak and subtracting that amount from the upper curvature peak. The middle 60% of the data between the two maxima in the curvature was used as it allowed for objective way to partition the phases while also providing a linear regression fit with R^2 values ≥ 0.99 for the first linear region. The second linear region was defined similarly; 20% of the time between the upper curvature peak and the end time was added to the upper curvature peak to define the start of the second linear region. This provided a linear regression fit with R^2 values ≥ 0.98. The first transition phase was defined as all data before the lower bound of the first linear region. This region shows additional curvature in some tests however this region contains few data points and is treated as a single transition phase in this analysis. The end of the first linear region and the start of the second linear region defined the second transition phase. Fig. 4 in the text shows the relationship between the curvature peaks and each defined phase.

Fig. 9 Curvature peaks for test 1a. Peaks marked with X are used for phase determination. Peaks within 0.5 log seconds from the start removed

Declarations

References

1. Fatoye, F., T. Gebrye, and I. Odeyemi. Real-world incidence and prevalence of low back pain using routinely collected data. *Rheumatol. Int.* 39:619–626, 2019. https://doi.org/10.1007/s00296-019-04273-0.

2. Murray, C. J., R. M. Barber, K. J. Foreman, A. A. Ozgoren, F. Abd-Allah, S. F. Abera, V. Aboyans, J. P. Abraham, I. Abubakar, and L. J. Abu-Raddad. Global, regional, and national disability-adjusted life years (DALYs) for 306 diseases and injuries and healthy life expectancy (HALE) for 188 countries, 1990–2013: quantifying the epidemiological transition. *Lancet.* 2015. https://doi.org/10.1016/S0140-6736(15)61340-X.

3. Okunribido, O. O., M. Magnusson, and M. H. Pope. Low back pain in drivers: the relative role of whole-body vibration, posture and manual materials handling. *J. Sound Vib.* 2006. https://doi.org/10.1016/j.jsv.2006.06.007.

4. Cole, M. H., and P. N. Grimshaw. The biomechanics of the modern golf swing: implications for lower back injuries. *Sports Med.* 2016. https://doi.org/10.1007/s40279-015-0429-1.

5. Trompeter, K., D. Fett, and P. Platen. Prevalence of back pain in sports: a systematic review of the literature. *Sports Med.* 2017. https://doi.org/10.1007/s40279-016-0645-3.

6. To, D., M. Rezai, K. Murnaghan, and C. Cancelliere. Risk factors for low back pain in active military personnel: a systematic review. *Chiropr. Man. Ther.* 2021. https://doi.org/10.1186/s12998-021-00409-x.

7. Knezevic, N. N., K. D. Candido, J. Vlaeyen, J. Zundert, and S. Cohen. Low back pain: epidemiology, mechanisms, and treatment. *Lancet.* 2021. https://doi.org/10.1016/S0140-6736(21)00733-9.

8. Koes, B. W., M. W. van Tulder, and S. Thomas. Diagnosis and treatment of low back pain. *BMJ.* 2006. https://doi.org/10.1136/bmj.332.7555.1430.

9. Urits, I., A. Burshtein, M. Sharma, L. Testa, P. A. Gold, V. Orhurhu, O. Viswanath, M. R. Jones, M. A. Sidransky, B. Spektor, and A. D. Kaye. Low back pain, a comprehensive review: pathophysiology, diagnosis, and treatment. *Curr Pain Headache Rep.* 2019. https://doi.org/10.1007/s11916-019-0757-1.

10. McMorran, J. G., and D. E. Gregory. The influence of axial compression on the cellular and mechanical function of spinal tissues; emphasis on the nucleus pulposus and annulus fibrosus: a review. *J. Biomech. Eng.* 2021. https://doi.org/10.1115/1.4049749.

11. Adams, M. A. Biomechanics of back pain. *Acupunct. Med.* 2004. https://doi.org/10.1136/aim.22.4.178.

12. Battié, M. C., T. Videman, L. E. Gibbons, H. Manninen, K. Gill, M. Pope, and J. Kaprio. Occupational driving and lumbar disc degeneration: a casecontrol study. *Lancet.* 2002. https://doi.org/10.1016/S0140-6736(02)11399-7.

13. Schmidt, A. L., G. Paskoff, B. S. Shender, and C. R. Bass. Risk of lumbar spine injury from cyclic compressive loading. *Spine.* 2012. https://doi.org/10.1097/BRS.0b013e3182752a19.

14. Gooyers, C. E., R. D. McMillan, S. J. Howarth, and J. P. Callaghan. The impact of posture and prolonged cyclic compressive loading on vertebral joint mechanics. *Spine.* 2012. https://doi.org/10.1097/BRS.0b013e318256f9e6.

15. Zehr, J. D., J. M. Barrett, and J. P. Callaghan. Cyclic loading history alters the joint compression tolerance and regional indentation responses in the cartilaginous endplate. *J. Mech. Behav. Biomed. Mater.* 2022. https://doi.org/10.1016/j.jmbbm.2022.105542.

16. Bass, C., R. Salzar, Z. Ziemba, S. Lucas, and R. Peterson. The modeling and measurement of humans in high speed planing boats under repeated vertical impacts. *Int. Res. Conf. Biomech. Impact.* 2005:10, 2005.

17. Adams, M., and W. Hutton. The effect of posture on the fluid content of lumbar intervertebral discs. *Spine.* 1983. https://doi.org/10.1097/00007632-198309000-00013.

18. Hedman, T. P., and G. R. Fernie. Mechanical response of the lumbar spine to seated postural loads. *Spine.* 1997. https://doi.org/10.1097/00007632-199704010-00004.

19. Gunning, J. L., J. P. Callaghan, and S. M. McGill. Spinal posture and prior loading history modulate compressive strength and type of failure in the spine: a biomechanical study using a porcine cervical spine model. *Clin. Biomech.* 2001. https://doi.org/10.1016/s0268-0033(01)00032-8.

20. Gallagher, S., W. S. Marras, A. S. Litsky, and D. Burr. Torso flexion loads and the fatigue failure of human lumbosacral motion segments. *Spine.* 2005. https://doi.org/10.1097/01.brs.0000182086.33984.b3.

21. Adams, M., and W. Hutton. The effect of posture on the lumbar spine. *J. Bone Joint Surg. Br.* 1985. https://doi.org/10.1302/0301-620X.67B4.4030863.

22. Gaydos, S. J. Low back pain: considerations for rotary-wing aircrew. *Aviat. Space Environ. Med.* 83:879, 2012.

23. Brinckmann, P., M. Biggemann, and D. Hilweg. Fatigue fracture of human lumbar vertebrae. *Clin. Biomech.* 1988. https://doi.org/10.1016/s0268-0033(88)80001-9.

24. Gallagher, S., and J. R. Heberger. Examining the interaction of force and repetition on musculoskeletal disorder risk: a systematic literature review. *Hum Factors.* 2013. https://doi.org/10.1177/0018720812449648.

25. Van Der Veen, A. J., M. G. Mullender, I. Kingma, and T. H. Smit. Contribution of verftebral bodies, endplates, and intervertebral discs to the compression creep of spinal motion segments. *J. Biomech.* 2008. https://doi.org/10.1016/j.jbiomech.2008.01.010.

26. Kazarian, L. E. Creep characteristics of the human spinal column. *Orthop. Clin. North Am.* 6:3, 1975.

27. Adams, M. A., and P. J. Roughley. What is intervertebral disc degeneration, and what causes it? *Spine.* 2006. https://doi.org/10.1097/01.brs.0000231761.73859.2c.

28. Wang, Y., T. Videman, and M. C. Battié. ISSLS prize winner: lumbar vertebral endplate lesions: associations with disc degeneration and back pain history. *Spine.* 2012. https://doi.org/10.1097/BRS.0b013e31824dd20a.

29. O'Connell, G. D., N. T. Jacobs, S. Sen, E. J. Vresilovic, and D. M. Elliott. Axial creep loading and unloaded recovery of the human intervertebral disc and the effect of degeneration. *J. Mech. Behave. Biomed. Mater.* 2011. https://doi.org/10.1016/j.jmbbm.2011.02.002.

30. Keller, T., D. Spengler, and T. Hansson. Mechanical behavior of the human lumbar spine. I. Creep analysis during static compressive loading. *J. Orthop. Res.* 1987. https://doi.org/10.1002/jor.1100050402.

31. Hansson, T., T. Keller, and D. Spengler. Mechanical behavior of the human lumbar spine. II. Fatigue strength during dynamic compressive loading. *J. Orthop. Res.* 1987. https://doi.org/10.1002/jor.1100050403.

32. Berger-Roscher, N., G. Casaroli, V. Rasche, T. Villa, F. Galbusera, and H. J. Wilke. Influence of complex loading conditions on intervertebral disc failure. *Spine*. 2017. https://doi.org/10.1097/BRS.0000000000001699.

33. Schmidt, A. L. Assessing the Injury Tolerance of the Human Spine. Durham: Duke University, 2017.

34. Wojtków, M., M. Głowacki, and C. Pezowicz. Multiscale structural characterization of the vertebral endplate in animal models. *J. Anat.* 2021. https://doi.org/10.1111/joa.13402.

35. King, J., and R. Roberts. Carcass length in the bacon pig; its association with vertebrae numbers and prediction from radiographs of the young pig. *Anim. Prod.* 1960. https://doi.org/10.1017/S0003356100033493.

36. Byrne, R. M., A. K. Aiyangar, and X. Zhang. A dynamic radiographic imaging study of lumbar intervertebral disc morphometry and deformation in vivo. *Sci. Rep.* 2019. https://doi.org/10.1038/s41598-019-51871-w.

37. Morino, C. F., S. T. Middleton, E. Dimbath, J. Op't Eynde, J. R. Kait, and C. R. Bass, Modelling viscoelastic creep response of porcine lumbar spinal units exposed to repeated flexion-compression loading. Cambridge, UK, 2023.

38. Morino, C., A. Schmidt, E. Dimbath, S. Middleton, J. Kait, J. Shridharani, M. Ortiz-Paparoni, J. Klinger, J. Op't Eynde, and C. Bass. Human and porcine lumbar endplate injury risk in repeated flexion-compression. *Ann. Biomed. Eng.* 2023. https://doi.org/10.1007/s10439-024-03508-x.

39. Dimbath, E., C. Morino, S. Middleton, J. Kait, and C. R. Bass. Lumbar Response to Flexion-Compression in Cyclic and Quasi-Static Loading in Intervertebral Discs. Cambridge: IRCOBI, 2023.

40. Karajan, N. Multiphasic intervertebral disc mechanics: theory and application. *Arch. Comput. Methods Eng.* 2012. https://doi.org/10.1007/s11831-012-9073-1.

41. Adams, M., P. Dolan, and W. Hutton. Diurnal variations in the stresses on the lumbar spine. *Spine*. 1987. https://doi.org/10.1097/00007632-198703000-00008.

42. Schmidt, H., C. Schilling, A. L. P. Reyna, A. Shirazi-Adl, and M. Dreischarf. Fluid-flow dependent response of intervertebral discs under cyclic loading: on the role of specimen preparation and preconditioning. *J. Biomech.* 2016. https://doi.org/10.1016/j.jbiomech.2015.10.029.

43. Little, J. S., and P. S. Khalsa. Human lumbar spine creep during cyclic and static flexion: creep rate, biomechanics, and facet joint capsule strain. *Ann Biomed Eng*. 2005. https://doi.org/10.1007/s10439-005-1742-x.

44. Rasoulian, A., F. Vakili-Tahami, and T. H. Smit. Linear and nonlinear biphasic mechanical properties of goat IVDs under different swelling conditions in confined compression. *Ann. Biomed. Eng.* 2021. https://doi.org/10.1007/s10439-021-02856-2.

45. Stokes, I. A., and J. C. Iatridis. Mechanical conditions that accelerate intervertebral disc degeneration: overload versus immobilization. *Spine*. 2004. https://doi.org/10.1097/01.brs.0000146049.52152.da.

46. Paul, C. P., T. Schoorl, H. A. Zuiderbaan, B. Zandieh Doulabi, A. J. van der Veen, P. M. van de Ven, T. H. Smit, B. J. van Royen, M. N. Helder, and M. G. Mullender. Dynamic and static overloading induce early degenerative processes in caprine lumbar intervertebral discs. *PloS ONE*. 2013. https://doi.org/10.1371/journal.pone.0062411.

47. Parkinson, R. J., and J. P. Callaghan. The role of dynamic flexion in spine injury is altered by increasing dynamic load magnitude. *Clin. Biomech.* 2009. https://doi.org/10.1016/j.clinbiomech.2008.11.007.

48. Callaghan, J. P., and S. M. McGill. Intervertebral disc herniation: studies on a porcine model exposed to highly repetitive flexion/extension motion with compressive force. *Clin. Biomech.* 2001. https://doi.org/10.1016/s0268-0033(00)00063-2.

49. Carter, D. R., W. E. Caler, D. M. Spengler, and V. H. Frankel. Fatigue behavior of adult cortical bone: the influence of mean strain and strain range. *Acta Orthop. Scand.* 1981. https://doi.org/10.3109/17453678108992136.

50. Vergroesen, P. A., A. J. van der Veen, K. S. Emanuel, J. H. van Dieën, and T. H. Smit. The poro-elastic behaviour of the intervertebral disc: a new perspective on diurnal fluid flow. *J. Biomech.* 2016. https://doi.org/10.1016/j.jbiomech.2015.11.041.